JOURNAL OF GEOPHYSICAL RESEARCH, VOL. 101, NO. B9, PAGES 20,449-20,466, SEPTEMBER 10, 1996

Strombolian explosions
2. Eruption dynamics determined from acoustic measurements

S. Vergniolle[1]

Institute of Theoretical Geophysics, University of Cambridge, Cambridge, England

G. Brandeis[2] and J.-C. Mareschal[3]

Laboratoire de Dynamique des Systèmes Géologiques, Institut de Physique du Globe de Paris

Abstract. Strombolian activity consists of a series of explosions due to the breaking of a large overpressurized bubble at the surface of the magma column. Acoustic pressure due to sound waves has been measured and analyzed at Stromboli for more than 50 explosions. Three parts can be distinguished in the acoustic pressure waveform, which are related to the behavior of the bubble before, during, and after its bursting. Before the sharp rise in acoustic pressure, the signal is dominated by waves with a frequency of 2 Hz, which develop on the nose of the bubble. They produce sound in air by imposing a rapid motion to the interface, and one could detect a bubble travelling in the uppermost 30 m of the magma column. When the bubble reaches the air-magma interface, its strong vibration, driven by a large overpressure inside the gas, generates the main event with a frequency around 9 Hz. After the bubble has burst, kinematic waves of frequency around 4.5 Hz are the main source of sound. They develop at the surface of the magma left on the conduit side. The three types of motion, although determined independently, give consistent results. Furthermore, combining the results obtained for the two types of kinematic waves, the magma viscosity is estimated to be of 300 ± 65 Pa s, which is in good agreement with petrological constraints and corroborates the validity of our analysis. This suggests that acoustic measurements constitute a powerful tool in the understanding of eruption dynamics.

Introduction

Records of atmospheric pressure and seismicity have been used to constrain the mechanism of volcanic eruptions. Long-period seismic events recorded during eruptions, like at Mount St. Helens, were used to calculate the driving force [*Kanamori and Given*, 1982; *Kanamori et al.*, 1984]. Violent eruptions, like that of Mount Pinatubo (Philipines) in 1991, can excite atmospheric oscillations [*Kanamori and Mori*, 1992]. During the Mount St. Helens eruption, several acoustic modes propagating in the lower atmosphere were recognized on an array of sensitive microbarographs [*Donn and Balanchandran*, 1981; *Mikumo and Bolt*, 1985].

Hydrophones were used to locate and describe submarine volcanic activity in the Pacific [*Norris and Johnson*, 1969]. They also have been used in crater lakes to monitor activity of volcanoes [*Bercy et al.*, 1983; *Vandemeulebrouck et al.*, 1994]. More recently, measurements suggest that monitoring acoustic pressure in crater lakes might be used to forecast eruptions [*Vandemeulebrouck et al.*, 1994]. Studies of acoustic pressure recorded in air are sparse [*Machado et al.*, 1962; *Richards*, 1963; *Woulff and MacGetchin*, 1976; *Vergniolle and Brandeis*, 1994, this issue]. The first studies of acoustics used a rather restricted frequency band, above 50 Hz. However, most of the energy of Strombolian explosions is below 50 Hz [*Vergniolle and Brandeis*, 1994]. *Richards* [1963] compared the characteristic sounds produced by each type of volcanic activity. *Woulff and McGetchin* [1976] were the first to calculate gas velocity from the total acoustic power. Their analysis, tested on fumaroles emitted by the Acatenango volcano (Guatemala), suggested that Strombolian eruptions produce a dipolar radiation. A

[1]Now at Laboratoire de Dynamique des Systèmes Géologiques, Institut de Physique du Globe de Paris.

[2]Now at UMR 5562 CNRS, Groupe de Recherches de Géodésie Spatiale, Observatoire Midi-Pyrénées, Toulouse, France.

[3]Now at GEOTOP, Université de Québec à Montréal, Montréal, Quebec, Canada.

Paper number 96JB01925.
0148-0227/96/96JB-01925$09.00

recent study has, however, shown that the source of the sound at Stromboli is a monopole [*Vergniolle and Brandeis*, 1994]. More recently, the airborne structure of the sound at Stromboli, mainly in audible frequencies, was analyzed in great detail and explained by resonances in the magma column [*Buckingham and Garcés*, 1996].

Application of fluid mechanics to volcanic activity is even more recent. Most studies are focused on understanding the dynamics of volcanic plumes [e.g., *Wilson et al.*, 1978; *Kieffer and Sturtevant*, 1984; *Sparks*, 1986; *Woods*, 1988]. Models for basaltic eruptions are less common [e.g., *Wilson and Head*, 1981; *Jaupart and Vergniolle*, 1988; *Vergniolle and Jaupart*, 1990]. Field data are needed to test laboratory and numerical models of eruption dynamics. Stromboli is an excellent candidate to be a laboratory volcano for basaltic eruptions because of its permanent activity. It consists of a series of explosions, caused by the breaking of a large overpressurised bubble at the surface of the magma column [*Blackburn et al.*, 1976; *Wilson*, 1980]. All explosions present a similar pattern and have a regular intermittency, typical of a well-developed slug flow in which bubbles, almost as large as the volcanic conduit, rise before bursting at the surface [*Jaupart and Vergniolle*, 1988]. *Vergniolle and Brandeis* [1994, this issue] have interpreted sharp variations in acoustic pressure (Figure 1) as due to the vibration of these large bubbles at the surface of the magma column just before they burst.

These bubbles form at depth, probably in a shallow magma chamber [*Jaupart and Vergniolle*, 1988], a few hundred meters deep [*Giberti et al.*, 1992]. Because they rise at a rather slow velocity, ≈ 1.6 m s^{-1} if the volcanic conduit is ≈ 1 m in radius [*Wallis*, 1969], they are at shallow depths during the last few seconds before they reach the surface. Therefore their behavior should affect the nearby air-magma interface. Strong motions on this interface could radiate sound waves into air, which can be detected by monitoring acoustic pressure. Similarly, the study of acoustic pressure after the bubble has burst may provide additional information on the eruption dynamics. The aim of this study is thus to perform a quantitative analysis of the frequencies of the sound before and after the bubble has burst.

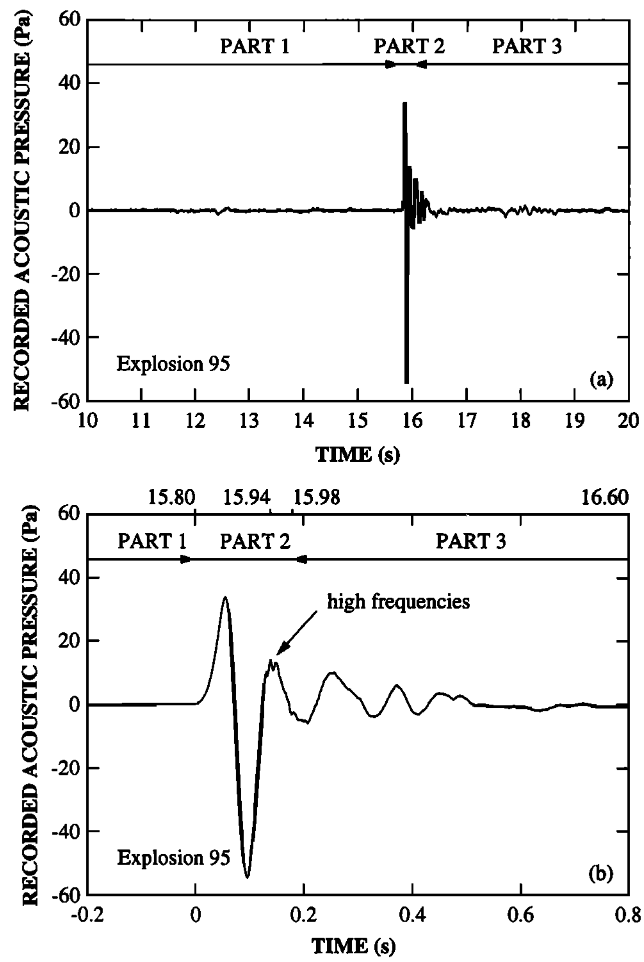

Figure 1. Waveform of explosion 95 ("1-Hz" microphone, high-frequency cutoff of 100 Hz). Onset of explosion is at 15.8 s. (a) Signal before and after the main event contains low frequencies. (b) Close-up of the waveform. The main event in acoustic pressure, from 15.8 to 15.98 s, is free of high frequencies and corresponds to the bubble vibration. High frequencies in the acoustic pressure, at 15.94 s, mark the bubble bursting.

General Features of Stromboli

Stromboli is a stratovolcano raising 3000 m above the seafloor to an elevation of 900 m above sea level, with two active craters at its summit (Figure 2). The western crater has one active vent, roughly elliptical (3 m $\times$ 1 m), with four explosions per hour on average [*Chouet et al.*, 1974]. The eastern crater is less active, with only one explosion per hour on average. From the five vents closely observed in September 1971, only one vent is well described, with a circular opening of roughly 0.5 m in diameter [*Chouet et al.*, 1974].

In April 1992, we could only see two or three vents inside the eastern crater, from a distance of 250 m. The lava in the western crater has been observed visually between explosions (P. Allard, personal communication, 1993). Bubbles of all sizes, from centimeters to a few meters, have been observed to break at the surface. For meter-size bubbles, the lava surface is strongly updomed by the arriving bubble which stays at the surface for less than a few seconds. Then the bubble breaks, sending fragments of a mean diameter of 2 cm [*Chouet et al.*, 1974] into the air and emitting sound at the same time. During explosions, ejecta are sent above the vent in a gas jet (80% H_2O, 10% CO_2, 5% SO_2, 5% Cl_2 (P. Allard, personal communication, 1993), at a few meters to 100 m high [*Weill et al.*, 1992], with velocities around 50 m s^{-1} [*Chouet et al.*, 1974; *Weill et al.*, 1992].

The present lava of Stromboli is a shoshonite [*Capaldi et al.*, 1978; *Francalanci et al.*, 1989]. From its composition, the viscosity of the lava can be estimated from both temperature and dissolved water content

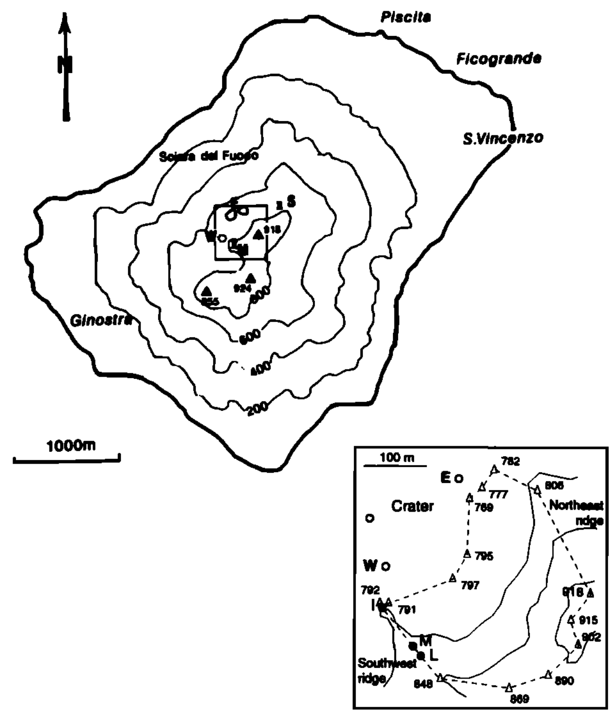

Figure 2. Map of Stromboli showing western crater (point W) and eastern crater (point E) and location of measurements (point M) with one microphone. The topography of the summit (square box) is adapted from [*Chouet et al.*, 1974; *Settle and McGetchin*, 1980]. Triangles represent points of known elevation [*Chouet et al.*, 1974]. When two microphones are used, DAT is at point M, the "4-Hz" microphone is at point I and the "1-Hz" microphone at point L on the southwest ridge.

[*Shaw*, 1972] or from its temperature only [*Bottinga and Weill*, 1972]. For the samples described by *Capaldi et al.* [1978] and *Francalanci et al.* [1989] and assuming no crystals, estimates range between 50 and 500 Pa s, for temperatures between 1273 K and 1373 K and water content between 0 wt% and 0.6 wt% [*Capaldi et al.*, 1978]. The phenocryst content is, however, highly variable, between 10 and 40% [*Francalanci et al.*, 1989]. Taking an average value of 20%, and following the *Roscoe* [1952] equation, the value of viscosity increases by a factor 2.5, giving a range of 125 to 1250 Pa s.

Stromboli has a low seismicity that has been attributed to the gas-magma dynamics in the uppermost portion of the magma column [*Ripepe et al.*, 1993, 1996]. Sharp and monochromatic seismic events, ≈ 2.5 Hz, in the western crater have been explained by a buried source [*Ripepe et al.*, 1993]. By contrast, the seismicity of the eastern vents is extremely shallow [*Ripepe et al.*, 1993]. For both craters, the volcano-seismic source is attributed to an explosion at the top of the magma column, generated by rising gas bubbles reaching the magma surface [*Braun and Ripepe*, 1993; *Ripepe et al.*, 1996], but the exact seismic signature of each vent is unknown [*Ntepe and Dorel*, 1990]. Measurements of seismic waves induced by explosions show that the first seismic waves at 1 Hz appear about 1 s before the second seismic waves, which contains two dominant frequencies at 2 and 5 Hz [*Lo Bascio et al.*, 1973; *Del Pezzo et al.*, 1992].

Acoustical Measurements

Experimental Setup

During 3 weeks in April 1992, acoustic measurements were performed on Stromboli volcano on a small crest close to the summit (Figure 2). Three different setups have been used. The first one, devoted to the waveform analysis, especially at low frequencies (1 Hz to 70 kHz), consists of a microphone (Bruel-Kjaer 4155), an amplifier (Bruel-Kjaer 2231), and a DAT recorder (Sony TCD-10 Pro) modified to accept low frequencies (-3 dB at 1 Hz). The second setup, used for the radiation pattern of the source, consists in two microphones, two amplifiers and two DAT recorders, at two different sites (points M and S, 250 and 370 m, respectively, from the eastern vents, on either side of the Stromboli summit, Figure 2). The second microphone (Bruel-Kjaer 4165) and amplifier (Bruel-Kjaer 2230) cover a narrower frequency range (4 Hz to 20 kHz). Each DAT has a time code in order to correlate arrival times. Finally, the third setup, used to locate the sources, connects the two pairs of microphones and amplifiers to the same DAT recorder. All instruments were calibrated with a sound level calibrator (Bruel-Kjaer 4230) of intensity 94 dB (rms pressure of 1 Pa) at 1000 Hz.

For all setups, the propagation from the vents toward the microphones is in direct line without any solid obstacle along the path. Although strongly dependent on humidity, the absorption coefficient in air is sufficiently small (10^{-3} dB m^{-1} [*Pierce*, 1981]) to be negligible, 0.25 dB at 250 m, before the 100 dB radiated by a small explosion. Therefore the acoustic pressure, measured in air with perfect weather conditions (dry, sunny, and without wind), is only due to the source. These experiments have shown that the source of sound radiates like a monopole, as the recorded intensity is inversely proportional to distance between vents and microphones.

The waveforms recorded by the "1-Hz" and "4-Hz" microphones are identical (Figure 3), allowing a precise determination of the delay in arrival time between them. Although the rough topography of the summit did not allow to vary much the emplacements of instruments, the distribution of the arrival time differences (Figure 3c) shows a scattering between 0.02 and 0.13 s, above the 0.02 s accuracy. This suggests that several vents are indeed active within the eastern crater, as observed by *Chouet et al.* [1974].

As shown by *Vergniolle and Brandeis* [this issue], the amplification of the sound by the upper part of the volcanic conduit can be ignored. In this paper, 36 explosions of the eastern vents recorded with the "1-Hz"

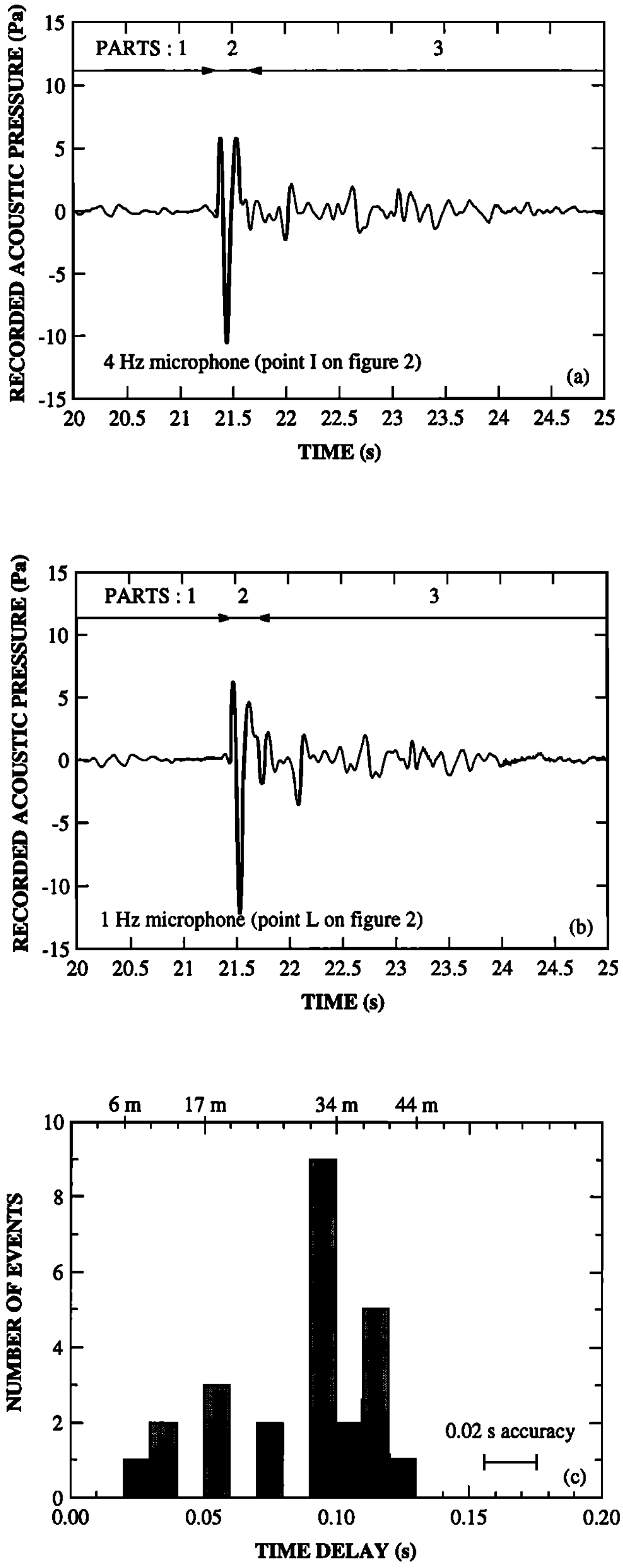

Figure 3. Explosion 775 at eastern vent, analyzed with a high-frequency cutoff of 100 Hz recorded simultaneously with: (a) the "4-Hz" microphone and (b) the "1-Hz" microphone. Open circle marks the onset of explosion, 21.35 s at point I and 21.44 s at point L. (c) Histogram of time delays between the two microphones for 25 explosions, giving path differences between 6 and 44 m (accuracy is of 0.02 s, about 7 m).

microphone have been selected for their good signal to noise ratio.

Frequency and Spectral Amplitude

All explosions exhibit the same waveform dominated by a sharp increase in acoustic pressure (Figure 1), called the main event, which is related to the strong vibration of the bubble before it burst [*Vergniolle and Brandeis*, this issue]. A spectrogram displays levels of the acoustic intensity as a function of time and frequency. The intensity I is given in decibels by

$$I = 20 \log \left(\frac{P_e}{P_{\text{ref}}} \right) \qquad (1)$$

where P_e is the measured effective pressure of the sound wave and P_{ref} is the reference effective pressure, 10^{-12} W m^{-2} for airborne sound [*Kinsler et al.*, 1982]. Looking at the spectogram outside the sharp rise in acoustic pressure (Figure 4) shows that the acoustic intensity can reach levels, 100–110 dB, as high as those generated by audible frequencies during the explosion. The purpose of this paper is therefore to study in detail the acoustic pressure before and after the sharp rise in acoustic pressure, as has been done for the main event itself by *Vergniolle and Brandeis* [this issue]. In the following, we call part 1 the signal before the sharp rise in amplitude, part 2 the sharp oscillation in pressure until high frequencies appear, and part 3 the reminding signal during the explosion (Figure 1).

The total acoustic power Π, in watts, emitted in a half sphere of radius equal to the distance r between the vents and the microphone, here 250 m, and radiated during a time interval T, is equal to

$$\Pi = \frac{\pi r^2}{\rho_{\text{air}} c T} \int_0^T |p_{\text{ac}} - p_{\text{air}}|^2 dt \qquad (2)$$

where $\rho_{\text{air}} = 1.1$ kg m^{-3} at 900 m elevation [*Batchelor*, 1967] and $c = 340$ m s^{-1} is the sound speed at the same elevation [*Lighthill*, 1978]. Although the acoustic pressure remains low in part 1 (Figure 1), the total acoustic power, calculated over a 5-s sliding window, shows an increase, by a factor 2, over $\approx$ 30 s which precedes the main event in part 2 (Figure 5a). Because this increase is shown by all explosions, we believe that acoustic pressure during part 1 is not a random noise but the consequence of a mechanism characteristic of the explosions at Stromboli. In keeping with the hypothesis that acoustic pressure during part 2 is generated by the bubble when it has reached the air-magma interface, we propose that acoustic pressure in part 1 records the last steps of the bubble rise in the magma column.

Examination of the spectrogram in part 1 suggests that bursts of energy ($100 \leq I \leq 110$ dB) occur every $\approx$ 2 s in signal, over more than 10 s, before the sharp rise in acoustic intensity (Figure 4). Although the cutoff

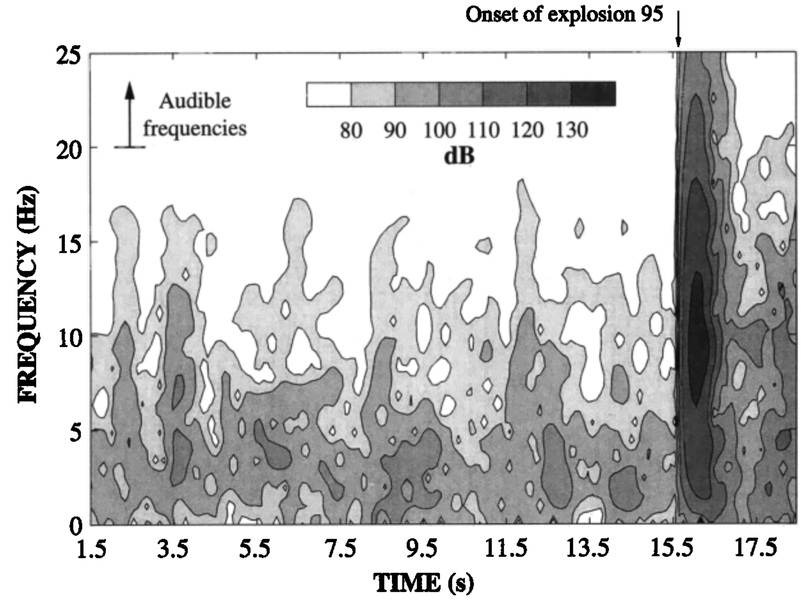

Figure 4. Spectrogram of explosion 95 (from eastern vents of Stromboli in 1992) from a sliding (0.2 s steps) time window of 3 s. Explosion 95 appears at 15.5 s with intensities above 130 dB at a frequency $\approx$ 9 Hz. Frequencies around 4.5 Hz are present before, with an intermittency of $\approx$ 2 s.

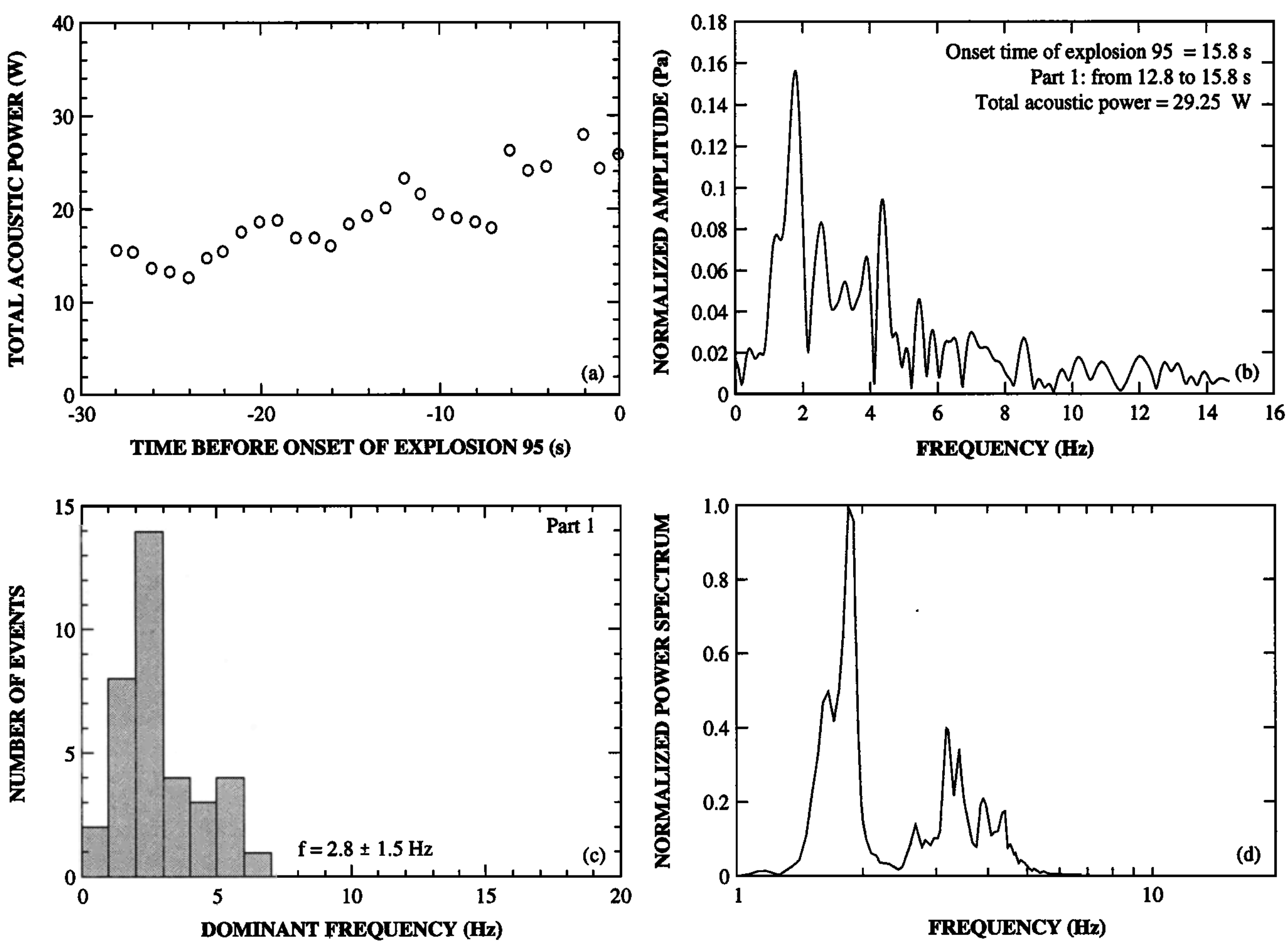

Figure 5. (a) Total acoustic power (W) as a function of time before the onset of explosion 95 and calculated for sliding windows of 5 s length. (b) Normalized amplitude during part 1 of acoustic pressure recorded during explosion 95 ("1-Hz" microphone, high frequency cutoff of 100 Hz, FFT was done on a 3-s time window padded with zeros up to 16384 points). (c) Histogram of dominant frequencies for the 36 explosions during the last 3 s of part 1. (d) Normalized power spectrum of ground velocity during a explosion quake (by courtesy of *Dietel et al.* [1994]).

frequency of our instrument is 1 Hz, this intermittency could be due to real oscillations at a frequency of ≈ 0.5 Hz. A recent seismic study at Stromboli [*Neuberg et al.*, 1994] has indeed shown the existence of frequencies below 1 Hz.

Part 1 has a characteristic spectral signature, with a dominant peak around 2 Hz and a secondary one around 4.5 Hz (Figures 5b and 5c). The overall shape of the power spectrum is strikingly similar to that obtained by *Dietel et al.* [1994] by stacking 45 vertical seismograms recorded early May 1992 (Figure 5d).

Similar to the total acoustic power, the amplitude of the ≈ 2 Hz peak increases during part 1 by a factor of 3 over the last 20 s or so before the beginning of part 2 (Figure 6a). It reaches its maximum, 0.16 ± 0.09 Pa, during the last 3 s before the onset of explosion (Figure 6b). This suggests that the source of the ≈ 2 Hz mode is the bubble itself during the last tens of meters of its rise in the magma conduit. More precisely, a 1-m radius bubble rises at ≈ 1.6 m s^{-1} [*Wallis*, 1969]. Therefore one could "hear" a bubble travelling in the uppermost 30 m of the magma conduit.

Part 2 is dominated by a strong maximum, $I \geq 130$ dB, at ≈ 9 Hz (Figure 4), with a possible secondary one near 4.5 Hz (Figures 6c and 6d). Because it is almost a transient, it contains a broad range of frequencies. Although the resolution is poor at low frequencies because of the short duration of part 2, the frequency analysis over a longer time interval (3 s, Figure 7a) suggests that this 4.5 Hz mode is indeed present.

Part 3 starts at the appearence of higher frequencies when acoustic pressure has returned to positive values after a strong negative peak (Figure 1b). It is characterized by a wider range of frequencies, between 1 and 10 Hz, with higher spectral amplitudes around 2, 4.5, and 9 Hz (Figures 7b and 7c). Note that these frequencies are those observed in parts 1 and 2. Comparison of power spectra (Figures 5b, 6c, 7a, and 7b) shows that the relative spectral amplitude of the 4.5-Hz mode increases until it becomes dominant in part 3.

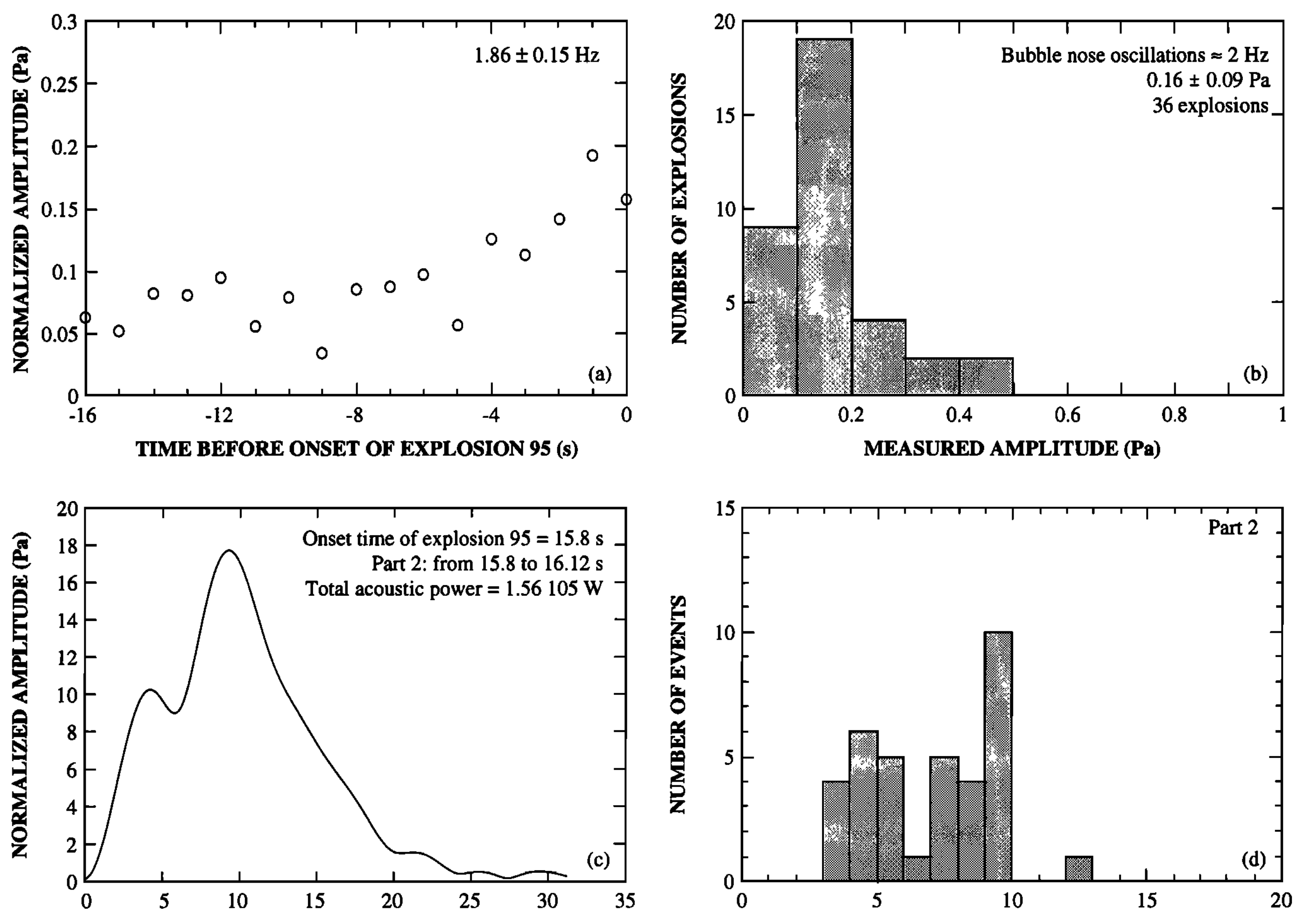

Figure 6. (a) Increase of amplitude (Pa) of the ≈ 2 Hz mode when approaching the onset of explosion 95. It is measured on FFT performed on sliding windows of 3 s length. (b) Measured amplitude of the bubble nose oscillations, at ≈ 2 Hz, 0.16 ± 0.09 Pa for 36 explosions. (c) Normalized amplitude (Pa) during part 2 of acoustic pressure recorded during explosion 95 (same characteristics as in Figure 5a). (d) Histogram of dominant frequencies for the 36 explosions during part 2.

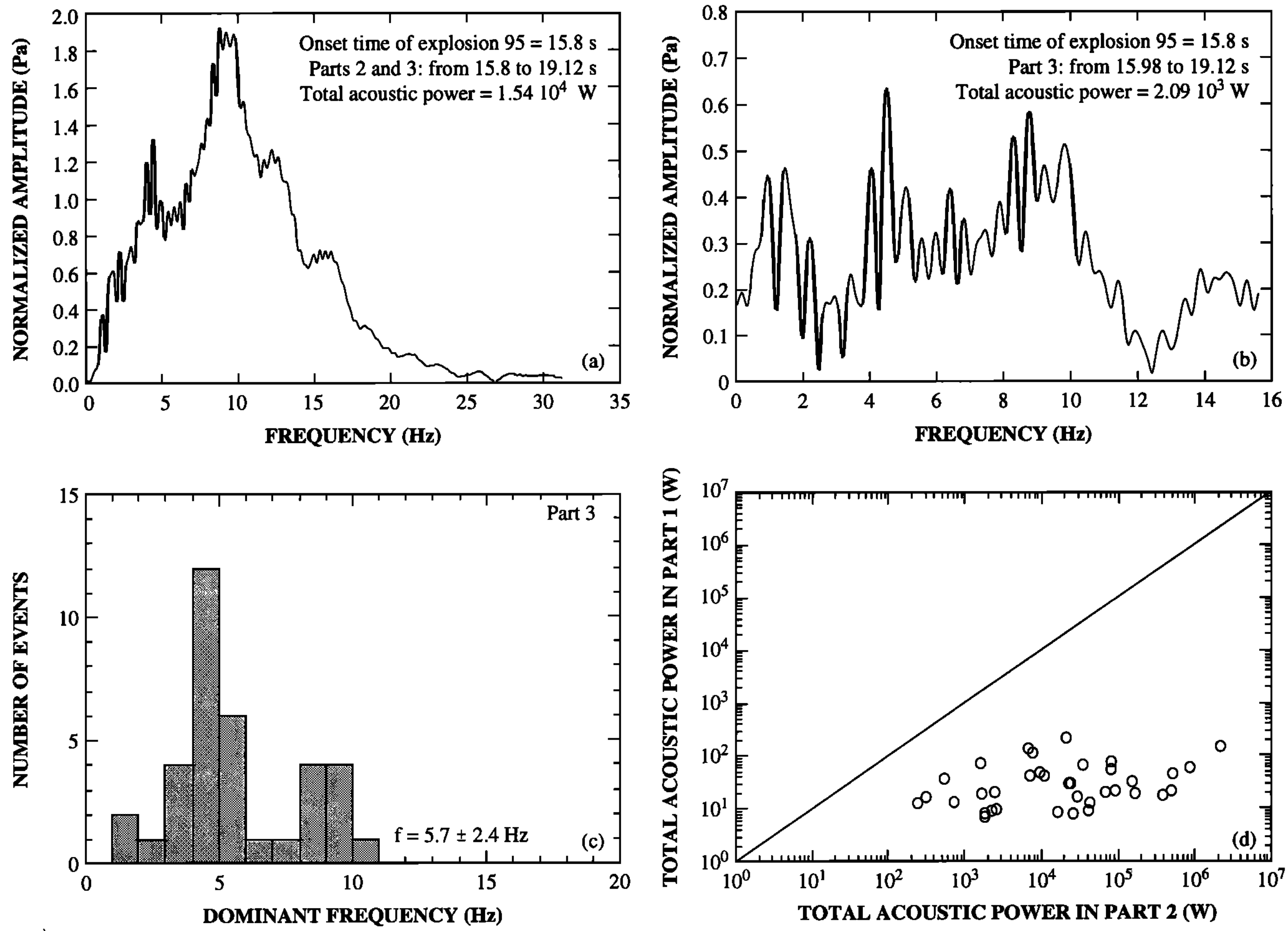

Figure 7. (a) Normalized amplitude during parts 2 and 3 combined of acoustic pressure recorded during explosion 95 (same characteristics as in Figure 5a). (b) same as in Figure 7a but during part 3. (c) Histogram of dominant frequencies for the 36 explosions during part 3. (d) Total acoustic power in part 1 versus total acoustic power in part 2.

The three parts have very different levels of acoustic power. The total acoustic power released during part 1 is between 1 and 200 W, comparable to the average thermal power released between explosions [*Gaonac'h et al.*, 1994]. During part 2, the total acoustic power is much larger, between 10^2 and 10^6 W (Figure 7d), 10^4 times more, on the average than during part 1. The acoustic power released during part 3 is intermediate between that of part 1 and part 2 (Figures 5b, 6c, 7a, and 7b).

Audible Sounds

One of the most spectacular effects of a volcanic eruption is the sound that can be heard, even at large distances. Audible sounds, above 20 Hz, recorded during parts 2 and 3 can have different origins. The main event (part 2), being a transient, contains a broad range of frequencies and, in particular, audible frequencies. Numerous collisions between solid walls and the ejecta, after the bubble bursting, could produce higher frequencies than those produced by the bubble vibration because ejecta are much smaller, less than 30 cm [*Chouet et al.*, 1974], than the average bubble size ($\approx$ 1 m). When ejecta hit the ground, they emit sounds like those produced by raindrops, which is a complex source of sound at audible frequencies [*Leighton*, 1994]. Finally, the expansion of a slightly overpressurized gas jet produces sound of wavelength the size of the eddies present in the turbulent jet [*Lighthill*, 1978]. Since eddies are smaller than the tube dimension, the expanding jet might also contribute to audible sounds. Audible sounds do not, however, contribute significantly to the acoustic pressure (Figures 5b, 6c, 7a, and 7b). Their acoustic intensity is around 100 dB (Figure 4) certainly powerful but still 30 times lower than the maximum intensity, 130 dB (equation (1)), of lower frequencies emitted during an explosion (Figure 4). Although striking, audible sounds are therefore not the most representative feature of Strombolian explosions.

Possible Sources of Sound

The frequency analysis has shown that parts 1, 2, and 3 are characterized by a particular frequency, which is natural to relate to a specific mechanism. The very existence of large bubbles [*Blackburn et al.*, 1976; *Wilson*, 1980], also overpressurized [*Vergniolle and Brandeis*, this issue] leads us to propose that all these mechanisms are related to the behavior of the bubble and its consequences on the surrounding magma.

Longitudinal Oscillations for a Rising Bubble

When gas pockets form at depth by coalescence of a foam layer [*Jaupart and Vergniolle*, 1989], they are overpressurized by the release of surface tension from the numerous small bubbles [*Vergniolle and Brandeis*, this issue]. The overpressure in the large bubble will force it to grow and oscillate, as observed in underwater explosion [*Taylor and Davies*, 1963]. Because the bubble cannot expand in width here, far from the air-magma interface, the oscillations will be longitudinal (Figure 8). Assuming that the magma layer above the bubble follows passively its motion, it may be considered as a mass attached to a vertically oscillating spring.

Assuming small oscillations and no damping, as by *Vergniolle and Brandeis* [1994], the radian frequency is the square root of the ratio between generalized stiffness and inertia, both derived from potential and kinetic energies, respectively [*Lighthill*, 1978]. Assuming for simplicity that the bubble is a cylinder of length L and radius R_o pushing a layer of magma of thickness H_l and density $\rho_l = 2700$ kg m^{-3}, the kinetic energy E_k of the oscillator is then

$$E_k = \frac{1}{2}(\pi \rho_l R_o^2 H_l)\dot{L}^2 \tag{3}$$

where $\dot{L} = dL/dt$ is the vertical velocity of the layer of magma and the term in parentheses is the generalized inertia. The potential energy for small oscillations is related to relative changes in gas density inside the bubble $\Delta\rho_g/\rho_{geq}$, which are equal to the relative changes in length $\Delta L/L_{eq}$, where index eq refers to equilibrium values. The potential energy E_p of the oscillator is then

$$E_p = \frac{1}{2}\left[\frac{\pi R_o^2 \gamma P_g}{L_{eq}}\right](\Delta L)^2 \tag{4}$$

where P_g is the pressure in the gas and γ is the ratio of specific heats, equal to 1.1 for hot gas [*Lighthill*, 1978]. The generalized stiffness is the term in square brackets in the expression of the potential energy. The frequency f_L of the oscillator is therefore

$$f_L = \frac{1}{2\pi}\sqrt{\frac{\gamma P_g}{\rho_l L_{eq} H_l}}. \tag{5}$$

It is clear that this calculation is only approximate because, in particular, the magma layer gets thinner as the bubble rises and increases in length by decompression. Keeping this in mind and setting P_g at the lithostatic value, the range of frequencies is from 0.4 Hz, for a 20-m-long bubble at a depth of 1 m, to 0.6 Hz for a 1-m-long bubble at a depth of 20 m, typical values of bubble lengths at Stromboli [*Vergniolle and Brandeis*, this issue]. Overpressure in the bubble would increase these values, but viscous dissipation in the magma layer would tend to decrease them. Although approximately

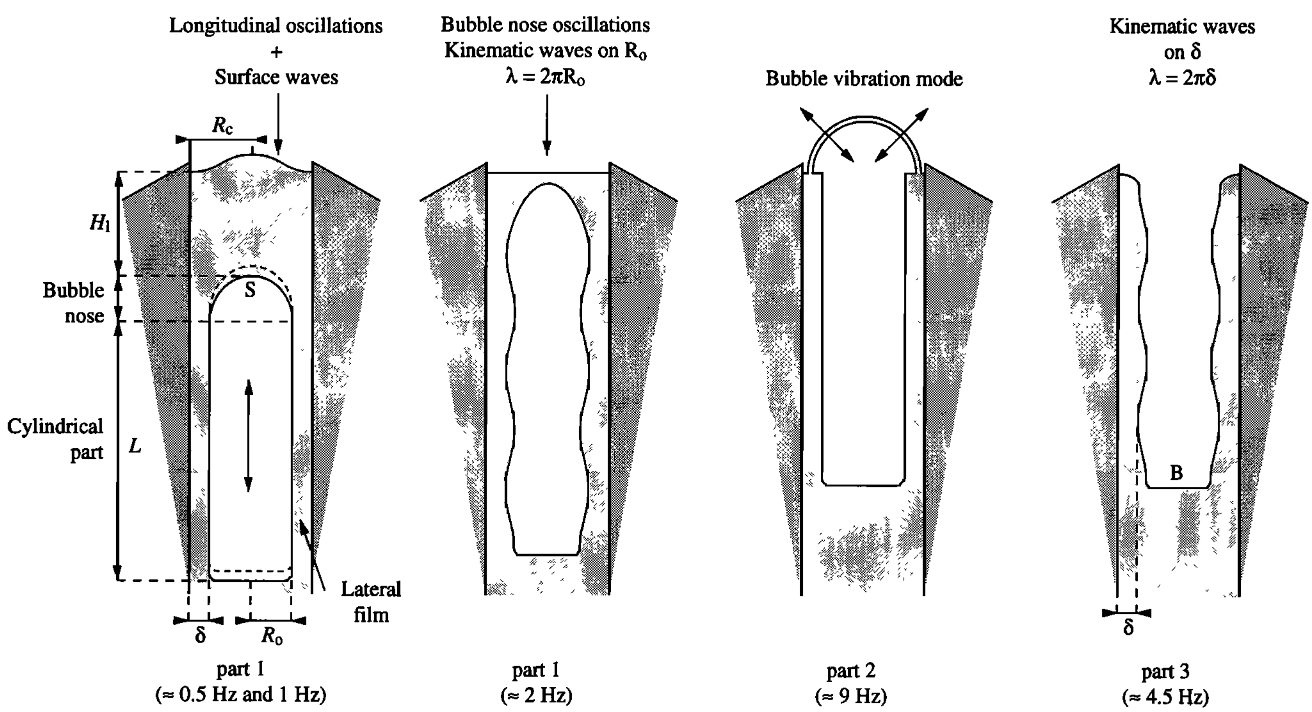

Figure 8. Sketches showing bubble motions responsible for frequencies measured during parts 1, 2, and 3. S (left) is a stagnation point at the tip of the bubble. B (right) is the bottom of the bubble. Other symbols are defined in text. The vertical arrow represents oscillations in the bubble length.

modeled, these longitudinal oscillations might explain the ≈ 0.5-Hz intermittency revealed by the spectrogram before the onset of explosion (Figure 4).

Kinematic Waves at the Nose of a Rising Bubble

We have considered so far that although its length could vary, the bubble kept a simple shape. Periodic changes in the bubble shape due to its overpressure [*Vergniolle and Brandeis*, this issue] could be the source of vibrations in the overlying magma layer and therefore be at the origin of fluctuations in the acoustic pressure in air. Two types of such changes in shape can be envisaged, one located at the nose and one on the sides of the bubble (Figure 8), each corresponding to a particular frequency.

When the overpressurised bubble arrives at shallow depths, the pressure difference between the top and the base of its cap becomes comparable to the general pressure field. This may force the tip of the bubble (S on Figure 8) to rise faster than the base of the cap, giving a pointy aspect to the bubble. The increase in length of the bubble nose will increase the downward velocity of the magma around the bubble and decrease the thickness of the lateral film (Figures 8 and 9) [*Batchelor*, 1967]. This will lead to an increase in dynamical pressure at the tip, thus forcing the nose to become flat again. Oscillations of the bubble shape will ensue, generating variations in thickness of the lateral film with the same frequency and wavelength as in the bubble nose.

Oscillations of the nose can then be understood as waves propagating at the gas-magma interface. Because magma is draining downward around the nose, the propagation of these waves is controlled by the drainage velocity. Assuming that drainage is laminar in a layer of thickness δ, V_{dr} is equal to

$$V_{\mathrm{dr}} = \frac{\rho_1 g \delta^2}{3\mu}. \tag{6}$$

For a viscous slug flow in a conduit of 1 m [*Chouet et al.*, 1974], δ is of the order of a few tens of centimeters. With a viscosity of a few hundreds pascal seconds, the Reynolds number in the lateral film is of the order of 10, small enough to justify our assumption of a laminar flow. Treating the magma around the bubble nose as a thin film, the velocity V_ω of these kinematic waves, which occur in systems where momentum can be neglected [*Wallis*, 1969; *Whitham*, 1973], is

$$V_\omega = 3V_{\mathrm{dr}} \tag{7}$$

where V_{dr} is the drainage velocity [*Wallis*, 1969]. Any change in the geometry of a hemisphere can be decribed by the superposition of various modes, analogous to spherical harmonics. The fundamental mode corresponds to a change in volume, from a hemispherical to a semiellipsoidal shape, preserving the cylindrical symmetry (Figure 9). While keeping a constant volume, higher modes distort the geometry. It is clear from Figure 9 that the mode of order n has a wavelength

$$\lambda_n = \frac{2\pi R_\mathrm{o}}{n}. \tag{8}$$

Even if all modes may be present in the early stages of the bubble evolution, the vertical pressure gradient will likely favor the odd modes, which preserve the cylindri-

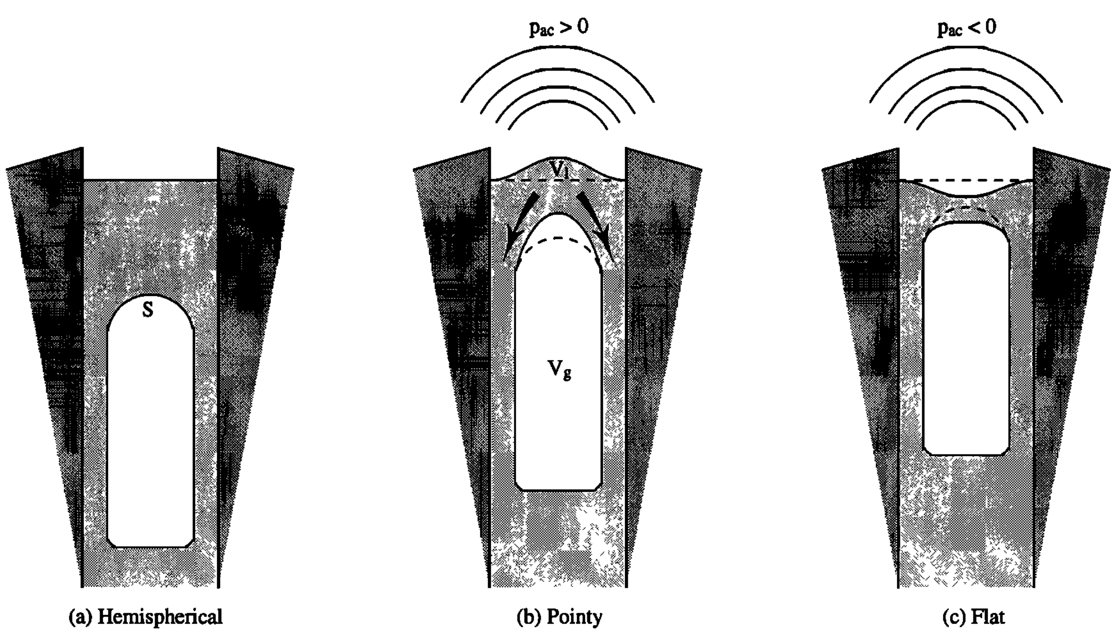

Figure 9. Sketch of bubble vibrations and consequent fluid motions during part 1 (see text for explanation).

cal symmetry, at the expense of the even modes which break the cylindrical symmetry. Combining equations (6), (7), and (8) gives the frequency of mode n

$$f_{nR_o} = \frac{n\rho_l g\delta^2}{2\pi\mu R_o} \tag{9}$$

with n being odd, as explained above. This relation shows that f_{nR_o} depends on the viscosity of the magma and of the film thickness δ which are not precisely known. For a bubble far from the interface, the minimum thickness of the lateral film in a slug flow, called the asymptotic thickness [*Batchelor*, 1967], is given by

$$\delta_\infty = 0.9R_o\left(\frac{\mu^2}{\rho_l^2 R_o^3 g}\right)^{\frac{1}{6}}. \tag{10}$$

Setting $\delta = \delta_\infty$ in equation (9) and eliminating δ_∞ between equations (9) and (10) gives

$$f_{nR_o} = \left[\frac{(0.9)^6 n^3}{8\pi^3}\frac{\rho_l g^2}{\mu}\right]^{\frac{1}{3}}. \tag{11}$$

Equation (11) shows that the $\approx$ 2-Hz frequency can be generated by the fundamental mode ($n = 1$) for a viscosity of 100 Pa s, and by the third mode ($n = 3$) for a viscosity of 2700 Pa s, much higher than any estimate at Stromboli (see above). Considering that the asymptotic thickness is seldom achieved, even for long bubbles [*Fabre and Linné*, 1992], the viscosity of 100 Pa s is certainly a lower bound in our framework, although it is the accepted value at Stromboli [*Blackburn et al.*, 1976]. Therefore we can exclude that the $\approx$ 2-Hz frequency is generated by the third order mode. Considering the same value for the viscosity, the third mode has a frequency of 54 Hz, which is not observed as an energetic mode in our acoustic records (Figures 5b, 6c, 7a, and 7b). The frequency of $\approx$ 2 Hz recorded in part 1 of acoustic pressure is therefore compatible with oscillations of the nose of the rising bubble. It remains to be shown that oscillations of the bubble nose can be transmitted as sound waves propagating in air when the bubble approaches the air-magma interface.

Acoustic Coupling of the Bubble Nose Oscillation for a Rising Bubble

The magma above the rising bubble being incompressible for low frequencies, any change in bubble volume, due to its overpressure [*Vergniolle and Brandeis*, this issue], is transmitted as a motion of the nearby air-magma interface with the same frequency: while in expansion the pointy bubble distorts the interface upward, during contraction the flat bubble pulls the free surface of magma downwards (Figures 8 and 9). At the same time, the lateral film is thinner for a pointy bubble, which enhances drainage around the bubble, and thicker for a flat bubble as shown for potential flow [*Batchelor*, 1967]. However, the variations in thickness of the lateral film produced by the change between pointy and flat do not affect significantly the nearby air-magma interface. Here, we propose that changes in the shape of the air-magma interface around its flat equilibrium value are capable of producing sound waves. The volume V_l of the radiating body at time t is the space delimitated on one side by the flat interface at equilibrium and on the other side by its surface at time t (Figure 9): this volume V_l is zero for equilibrium, i.e., a flat interface, positive when the interface is above its equilibrium value and negative when it is below. These changes in volume around the air-magma interface radiate sound waves like a monopole source but in half a sphere of radius r, distance between the vent and the microphone. The excess in acoustic pressure $p_{ac} - p_{air}$ at time t is [*Lighthill*, 1978]

$$p_{ac} - p_{air} = \frac{d^2}{dt^2}\left[V_l(t - r/c)\right]\frac{\rho_{air}}{2\pi r} \tag{12}$$

where ρ_{air} is air density (1.1 kg m^{-3} at 900 m above sea level [*Batchelor*, 1967]), c is the sound speed at the same elevation (340 m s^{-1} [*Lighthill*, 1978]), and p_{air} is the atmospheric pressure, $\approx 10^5$ Pa. Because the magma is incompressible, all changes in the bubble volume V_g are entirely transmitted to changes in volume around the interface V_l, which gives

$$\begin{aligned}\frac{d^2}{dt^2}\left[V_l(t - r/c)\right] &= \frac{d^2}{dt^2}\left[V_g(t - r/c)\right] \\ &= 4\pi^2 V_{geq} f_{nR_o}^2 A\sin(\omega t + \phi)) \end{aligned} \tag{13}$$

when assuming small oscillations of amplitude A, frequency f_{nR_o} and phase ϕ for the bubble volume V_g and where indices eq and g stand for equilibrium values and gas, respectively. When the bubble is at its minimum volume, $V_g = V_{geq} - \Delta V$, its internal pressure is maximum, $P_g = P_{geq} + \Delta P$, where ΔP is the bubble overpressure, here assumed constant. It gives $A = \Delta V/V_{geq}$ and the maximum excess pressure p_{thR_o} becomes

$$p_{thR_o} = \frac{2\pi\rho_{air}\Delta V f_{nR_o}^2}{r}. \tag{14}$$

Assuming that the bubble nose oscillation is the only mode present before the onset of explosion (Figures 5b and 5c), variations in bubble volume ΔV are related to variations in pressure ΔP through the adiabatic law by

$$P_{geq}V_{geq}^\gamma = (P_{geq} + \Delta P)(V_{geq} - \Delta V)^\gamma. \tag{15}$$

Because the deformations of the bubble nose occur at a velocity 3 times higher than the drainage in the lateral film (equation (7)), the latter can be neglected on the average during one cycle of vibration. The equilibrium pressure in the bubble P_{geq} is simply the weight of the overlying magma of thickness H_l. If we assume that the rise speed of the bubble U_b is also constant on the average over one cycle, $\approx$ 1.55 m s^{-1} for a tube of 2 m in diameter [*Wallis*, 1969], the pressure in the bubble P_g varies in time as

$$P_{geq} = \rho_l g(H_{lo} - U_b t) + P_{air} \tag{16}$$

where H_{lo} is the thickness of the magma layer of density ρ_l at time $t = 0$ and P_{air} the atmospheric pressure $\approx 10^5$ Pa.

The maximum amplitude radiated by the bubble nose oscillations in part 1 of acoustic pressure can be calculated from equation (14) for the 36 explosions. Taking estimates of bubble radius, length and overpressure determined from the bubble vibration mode [*Vergniolle and Brandeis*, this issue], and the average value of 2 Hz as the frequency of the bubble nose oscillations (Figures 5b and 5c), we obtain a theoretical value of a few tenths of a pascal (0.36 ± 0.30 Pa), the same order of magnitude as for measured amplitudes, 0.16 ± 0.09 Pa (Figure 6b).

The theoretical amplitude is slightly larger than the measured one, but our calculations rely on several assumptions. First, we have assumed for simplicity that the entire bubble overpressure triggers oscillations in the bubble nose. However, the bubble overpressure could also excite regular variations in the bubble length, a mode of very low frequency, ≈ 0.5 Hz. Therefore this latter mode can remove some of the energy driving the oscillations of the bubble nose at ≈ 2 Hz. Second, the viscosity of magma above the bubble might add another significant source of energy dissipation. Hence we suggest that the oscillation of the bubble nose is the main mechanism present during the rise of the bubble, part 1 of acoustic pressure, although it may be sometimes partially weakened by a different process such as the oscillations of the bubble length.

Surface Waves at the Air-Magma Interface

Finally, the last mechanism that can be envisionned during the last stage of the bubble ascent toward the top of the magma column is the deformation at the surface of the nearby air-magma interface. More generally, the motion of the air-magma interface can be described as the superposition of a global up-and-down motion and more complex deformations which can be interpreted as surface gravity waves, in a way analogous to sloshing in a cylindrical container. Two types of motion occur, one with pure radial dependence and one with angular dependence [*Paterson*, 1983]. When the depth of the container is larger than two thirds of its radius and assuming a potential flow, the frequency f_g is

$$f_g = \frac{1}{2\pi}\sqrt{gk} \tag{17}$$

where k is the wavenumber and g is the acceleration of gravity [*Paterson*, 1983]. If R_c is the radius of the container, the first radial modes have a wavenumber such that $kR_c/\pi = 1.2197, 2.2330, 3.2383 \cdots$ [*Paterson*, 1983]. For a tube of radius equal to 1 m as for an average explosion [*Vergniolle and Brandeis*, this issue], corresponding frequencies are 0.98 Hz, 1.32 Hz, 1.59 Hz $\cdots$. For angular modes, the wavenumber k is such that $kR_c/\pi = 0.586, 1.697, 2.717 \cdots$, giving frequencies of 0.68 Hz, 1.2 Hz, 1.5 Hz $\cdots$ [*Paterson*, 1983]. Although difficult to quantify, the effect of viscosity in the magma layer would be to lower these values. This wide range of frequencies show that the conduit does not filter out the low frequencies generated by the bubble below. Furthermore, if the ≈ 2 Hz value is related to sloshing, it has to be an harmonic of either ≈ 0.98 Hz or ≈ 0.68 Hz. In this case, we would expect the fundamental to have more energy than the harmonic, which is not what we observe.

Therefore in acoustic pressure, part 1 is a superposition of the three mechanisms described above and generated by the rising bubble: probably the oscillation of the bubble length (≈ 0.5 Hz), almost certainly the oscillations of the bubble nose (≈ 2 Hz), and probably some of the sloshing modes (≈ 1 Hz). During the bubble rise at the vicinity of the surface, the oscillations of the bubble nose are driven by the overpressure; hence the ≈ 2 Hz is the most energetic mode in part 1. Furthermore, we have shown that its acoustic intensity is a significant measurement and that its amplitude can be theoretically reproduced.

Bubble Vibration Mode

As the bubble keeps rising, the magma layer above it gets thinner, to a point where the bubble can rise above the tube (Figure 8). There, strong radial motions of the bubble cap become possible, generating a new set of frequencies (Figures 6c and 6d), which are recorded in part 2. By fitting the waveform of the same 36 explosions [*Vergniolle and Brandeis*, this issue], we could constrain the bubble radius, the bubble length, and the internal overpressure to be 0.9 ± 0.3 m, 7.3 ± 3.0 m, and $2.0 \pm 1.8 \times 10^5$ Pa, respectively.

Kinematic Waves of the Lateral Film Thickness After Bubble Bursting

After the bubble has burst, most of the lateral film of magma remains in the conduit, as shown from the volume of ejecta [*Vergniolle and Brandeis*, this issue]. Then, the film of magma is drained down into the tube (Figure 10), as observed also in basaltic eruptions at Hawaii [*Swanson et al.*, 1971]. It is well known that except at really small Reynolds numbers, waves can develop at the surface of a thin vertical film [*Wallis*, 1969; *Whitham*, 1973]. Kinematic waves occur in fluids where gravity is balanced by drag forces, here due to the viscosity of the magma [*Wallis*, 1969; *Whitham*, 1973], as shown in laboratory experiments (Figure 10). Since the Reynolds number in the lateral film is of the order of 10 (see above), kinematic waves are likely to develop along the volcanic conduit at Stromboli. Here we propose that they are a possible source for the ≈ 4.5 Hz frequency

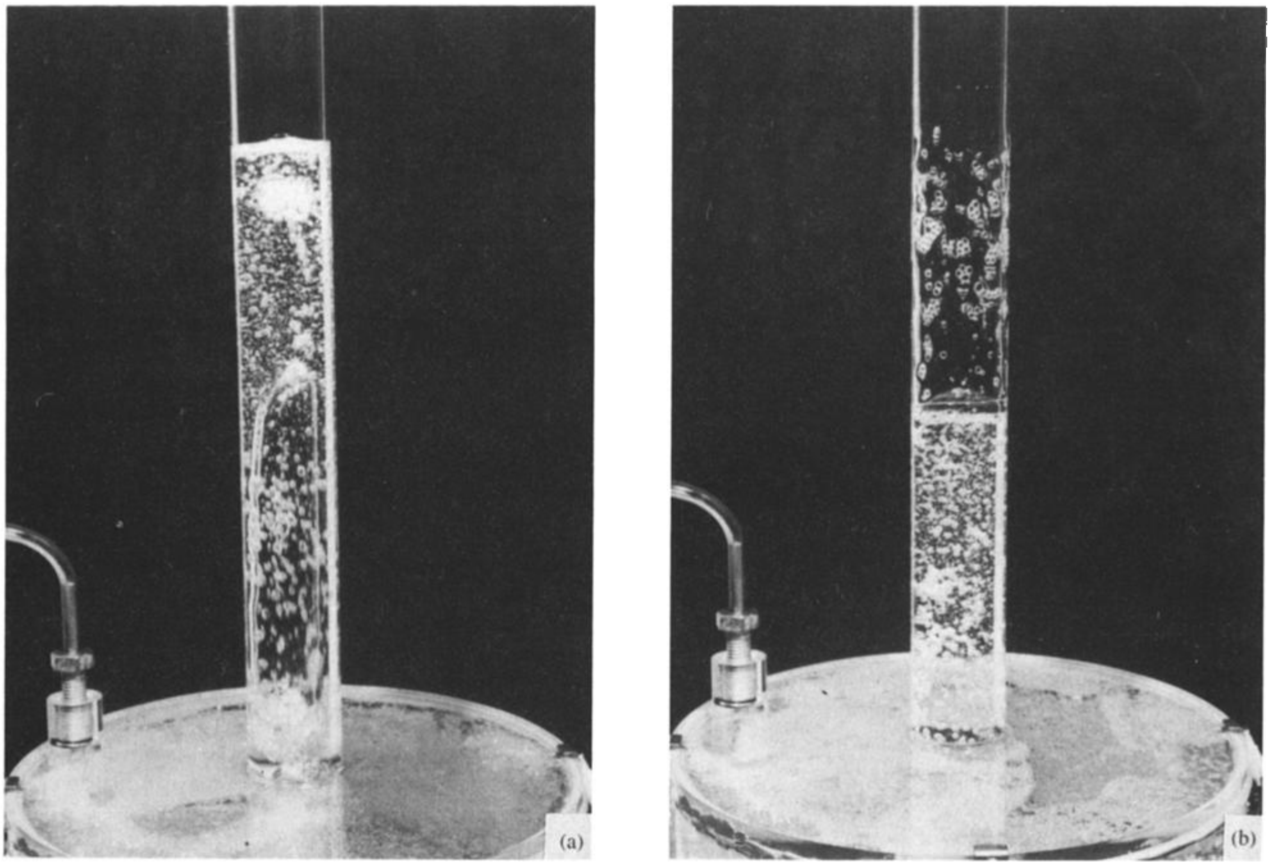

Figure 10. Experiments showing kinematic waves propagating along the vertical film of liquid. (a) During the bubble rise. (b) After the bubble has burst. Experiments were performed with a silicon oil of viscosity 0.1 Pa s and the tube was 4.4 cm in diameter.

recorded in part 3 of acoustic pressure (Figures 7b and 7c).

Our model implicitly assumes that the volcanic conduit is smooth, at least in its uppermost part. The almost continuous activity of the Stromboli for about 2000 years, with frequent and regular explosions, one per hour on average, has certainly eroded all major irregularities along the conduit surface. Besides, the delay between two explosions, $\approx$ 1 hour, is too short for the hot and rather fluid magma to leave solid fragments along the wall when it cools.

The angular frequency of kinematic waves is the ratio between the propagation velocity V_ω (see equation (7)) and a characteristic length of the phenomenon [*Landau and Lifschitz*, 1987]. Here, it is natural to take the thickness δ of the film as this characteristic length. Therefore the frequency $f_{k\delta}$ of these kinematic waves is

$$f_{k\delta} = \frac{\rho_l g \delta}{2\pi\mu} \tag{18}$$

and depends on the viscosity and on the thickness of the lateral film which are poorly constrained. Using as before the assymptotic value for the thickness of the lateral film δ_∞, the frequency $f_{k\delta}$ becomes

$$f_{k\delta} = \frac{0.9}{2\pi}\left(\frac{\rho_l}{\mu}\right)^{\frac{2}{3}} g^{\frac{5}{6}} R_\delta^{\frac{1}{2}}. \tag{19}$$

For a magma viscosity between 100 and 1000 Pa s as given from petrological constraints (see above), the frequency of kinematic waves $f_{k\delta}$ on the lateral film thickness is 4.9 ± 3 Hz, which is close to the last strong unexplained mode, $\approx$ 4.5 Hz, in part 3 of acoustic pressure. However, because of the strong dependence of $f_{k\delta}$ on the magma viscosity, which is poorly known, the exact frequency of these kinematic waves is difficult to calculate more accurately at this stage.

The variations in thickness of the lateral film, which are probably axisymetric, can be transmitted at the bottom of the bubble. Hence these packets of magma travel downward like evenly spaced rings along the wall of the conduit. When they arrive at the bottom of the bubble, they generate oscillations at the surface of the new air-magma interface with the same frequency (Figure 8). Then motions at the bottom can be described in terms of surface gravity waves for which a wide range of low frequencies can be produced. As for the oscillations at the bubble nose, the variations in the thickness δ of the lateral film correspond to changes in volume of the new air-magma interface around its flat equilibrium position at the bottom of the bubble. Hence as for the bubble nose oscillation, the excess in acoustic pressure is related to the second time derivative of the volume of the lateral film and is a monopole source (equation (12)). Assuming small oscillations in the thickness of the lateral film around its equilibrium value δ_o, δ becomes

$$\delta = \delta_o \left[1 + A \sin(2\pi f_{k\delta}\, t + \phi)\right] \tag{20}$$

where A is the normalized amplitude and ϕ is the phase. The variation in the elementary volume of liquid $dV_{l\delta}$ is

$$\frac{dV_{l\delta}}{dt} = 2\,\pi\, R_o\, \delta\, V_\omega \tag{21}$$

where the velocity of these kinematic waves is $V_\omega = 2\pi f_{k\delta}\, \delta$ (equation (7)) and giving

$$\frac{d^2}{dt^2}\left[V_{l\delta}\right] = 16\,\pi^3\, A\, R_o\, \delta_o^2\, f_{k\delta}^2\, \left[-\cos(2\pi f_{k\delta} t + \phi)\right] \cdot \tag{22}$$

As before (equation (12)), the maximum excess pressure $p_{\text{th}\delta}$ becomes

$$p_{\text{th}\delta} = \frac{8\,\pi^2\, \rho_{\text{air}}\, R_o\, \delta_o^2\, A\, f_{k\delta}^2}{r}. \tag{23}$$

Because the conditions on the lateral film when the bubble bursts are difficult to estimate, we cannot predict the amplitude A of these waves, except that they are probably small. Taking arbitrarily $A = 0.3$, $\delta_o = 0.6 R_o$ as predicted by theory [*Wallis*, 1969] and setting $f_{k\delta} \approx$ 4.5 Hz, the theoretical amplitude of these waves is 0.60 Pa for the average bubble radius $R_o = 0.9$ m [*Vergniolle and Brandeis*, this issue]. This is in very good agreement with the measured amplitude, 0.62 ± 0.35 Pa (Table 1). Therefore the mode at $\approx$ 4.5 Hz recorded in part 3 of acoustic pressure could be generated by kinematic waves of the lateral film thickness, and these waves are able to radiate sound at the measured levels. The presence of the $\approx$ 4.5-Hz frequency during part 1, albeit with an extremely low amplitude (Figure 5b), and which could not be explained by an harmonic of the bubble nose oscillations, suggests that this mechanism was already at work during the last stage of the bubble rise.

Application to Stromboli

Unlike for the $\approx$ 2-Hz mode, the strong dependence between magma viscosity and the frequency of kinematic waves on the lateral film thickness (equation (19)) has prevented us to show that they correspond to the $\approx$ 4.5-Hz mode recorded in part 3 of acoustic pressure, although we obtain a good order of magnitude for its amplitude. In the following, we reinforce this interpretation and show how to constrain independently the magma viscosity and the thickness of the lateral film.

Determination of Viscosity

The most energetic frequencies in parts 1 and 3 are 2.8 ± 1.5 Hz and 5.7 ± 2.4 Hz, respectively (Figures 5c and 7c). These modes show a wide scattering which may be interpreted in two different ways. The first one is to consider that all dominant frequencies are due to the same mechanism, oscillations of order 1 of the bubble nose and kinematic waves in part 3. The dispersion in frequencies would simply reflect a spread in contributing parameters, namely, bubble radius and viscosity. The distribution in time delays between the two microphones (Figure 3c) has indeed suggested that several vents are active within the eastern crater and there is no reason to think that all vents have identical radii.

For a well-developed slug flow in which the flow within the lateral film around the bubble is laminar, the theoretical thickness δ of the lateral film is shown to be 0.6 times the bubble radius [*Wallis*, 1969]. Taking estimates of the bubble radius given for each explosion by the bubble vibration mode during part 2 (Table 1), the 2.8 ± 1.5 Hz frequency of part 1 (Figure 5c) constrains the viscosity to be 600 ± 550 Pa s (Figure 11a), from equation (9). Similarly, the 5.7 ± 2.4 Hz frequency in part 3 gives, from equation (18), a viscosity of 400 ± 230 Pa s (Figure 11a). The range of viscosities compatible for both parts 1 and 3 is thus 400 ± 230 Pa s (Figure 11a) if ones takes the most energetic frequencies in parts 1 and 3 as due to oscillations of the bubble nose and to kinematic waves on the lateral film respectively.

The second way to interprete the scattering in frequencies (Figures 5c and 7c) is to consider that it results from the superposition of frequencies generated by at least two different mechanisms, as suggested by the amplitude spectrum of explosion 95 (Figures 5b and 7b). All explosions, except four, show two significant peaks of spectral amplitude during part 1 (Table 1). Guided by the example of explosion 95, we have selected the frequency that is closest to 2 Hz. For 26 explosions among 36, this frequency has the highest spectral amplitude (Table 1). This reduces the scattering to 2.2 ± 0.8 Hz. From equation (9) and again taking $\delta = 0.6\, R_o$ for each explosion [*Wallis*, 1969], the corresponding viscosity is of 650 ± 430 Pa s (Figure 11a).

In part 3, all explosions show three peaks in which the mode at $\approx$ 2 Hz is dominant for three explosions and the mode at $\approx$ 9 Hz for 10 explosions (Figure 7c and Table 1). For the remainding 23 explosions, the frequency of $\approx$ 4.5 Hz is the most energetic and for 12 others, it is among the three most energetic but not far from the maximum (Table 1). When selecting the mode closest to $\approx$ 4.5 Hz as representative of the kinematic waves, an average frequency of 4.5 ± 0.5 Hz is obtained. From equation (18), and again taking $\delta = 0.6\, R_o$ for each explosion, the viscosity is 420 ± 150 Pa s (Figure 11a), well within the range of values derived from part 1. Comparison between the different values of viscosity shows that the values derived from kinematic waves are better constrained and that the filtering of frequencies does not change much the viscosity. A range of 420 ± 150 Pa s would reconcile all interpretations in parts 1 and 3.

Table 1. Dominant Frequencies f in Decreasing Order of Spectral Amplitude A for Parts 1 and 3 and Bubble Radius R_o.

	Part 1				Part 3						
Explosion	f_1, Hz	A_1	f_2, Hz	A_2	f_1, Hz	A_1	f_2, Hz	A_2	f_3, Hz	A_3	R_o, m[a]
30	2.5	0.20	1.5	0.13	1.1	0.30	13.0	0.24	4.7	0.22	0.5
43	5.3	0.08	1.1	0.07	4.0	0.28	10.0	0.25	1.9	0.24	1.0
49	2.2	0.10	1.4	0.09	9.4	0.43	7.2	0.36	4.4	0.30	1.0
61	2.2	0.13	0.7	0.10	4.6	0.59	11.0	0.57	1.7	0.56	0.8
70	1.6	0.33	2.3	0.16	4.6	0.38	8.7	0.36	5.1	0.36	0.8
73	3.3	0.12	1.9	0.11	4.5	0.45	9.2	0.44	13.0	0.36	0.8
84	3.0	0.12	3.7	0.11	8.8	0.39	1.7	0.36	2.5	0.34	1.3
90	1.3	0.17	0.8	0.17	3.9	0.31	3.3	0.24	4.6	0.22	1.3
94	5.3	0.23	5.7	0.23	9.5	1.00	2.3	0.98	4.5	0.75	0.6
95	1.8	0.16	4.4	0.10	4.5	0.44	4.0	0.31	2.3	0.30	0.8
106	4.0	0.11	3.1	0.11	3.3	0.50	1.5	0.36	2.0	0.35	1.3
110	2.5	0.26	1.1	0.17	8.7	0.51	8.2	0.48	3.2	0.43	0.8
111	2.4	0.25	1.9	0.23	4.6	0.29	3.3	0.27	1.3	0.25	0.8
112	3.4	0.20	0.7	0.18	8.8	0.58	7.1	0.52	5.7	0.47	1.0
113	2.9	0.12	0.9	0.10	2.0	0.33	1.6	0.33	2.5	0.28	0.6
145	3.0	0.06	4.5	0.06	11.0	0.76	9.1	0.62	3.1	0.45	0.6
158	2.3	0.07	1.7	0.06	6.1	0.06	1.2	0.05	4.6	0.05	0.6
167	1.1	0.22	2.9	0.18	9.9	0.63	4.0	0.53	3.3	0.47	1.1
230	2.3	0.41	4.4	0.27	9.0	0.65	8.0	0.59	3.9	0.53	0.4
248	2.0	0.15	2.7	0.11	2.8	0.24	0.9	0.22	4.3	0.20	0.6
250	1.1	0.11	5.3	0.09	5.3	0.36	4.4	0.28	1.9	0.27	0.8
254	2.1	0.08	5.0	0.08	5.1	0.29	3.1	0.26	11.0	0.22	0.3
256	4.2	0.10	5.1	0.06	4.5	0.49	3.6	0.32	5.7	0.22	0.4
275	4.4	0.07	5.5	0.06	5.4	0.14	6.7	0.13	2.6	0.11	0.5
321	3.6	0.10	3.1	0.06	5.1	1.30	3.4	0.97	5.5	0.79	0.5
360	6.1	0.06	3.2	0.05	9.1	0.21	7.1	0.18	5.5	0.13	0.6
379	1.3	0.21	3.6	0.13	4.8	0.21	4.3	0.17	3.1	0.15	0.6
508	1.6	0.13	2.0	0.11	4.0	0.41	3.5	0.36	4.5	0.29	0.6
615	1.5	0.18	2.1	0.17	7.3	0.29	5.1	0.25	6.1	0.23	0.7
620	2.2	0.07	3.2	0.07	4.6	0.37	2.4	0.29	5.2	0.28	0.7
761	2.5	0.33	2.1	0.24	4.6	0.81	7.0	0.78	5.8	0.73	0.6
768	6.0	0.17	3.6	0.16	5.5	0.80	4.6	0.59	4.0	0.53	0.6
775	5.9	0.13	3.1	0.12	4.2	0.42	5.5	0.36	3.7	0.29	0.7
777	2.2	0.18	1.8	0.17	4.9	1.10	4.4	0.91	6.1	0.75	0.9
783	0.9	0.20	5.4	0.19	5.3	0.37	6.5	0.27	9.3	0.21	0.9
788	0.5	0.43	1.3	0.42	4.8	0.83	8.5	0.78	4.0	0.71	1.0

[a]Determined from *Vergniolle and Brandeis* [this issue] for the 36 explosions, assuming a film thickness of 2 cm above the bubble during part 2.

So far, parts 1 and 3 have been treated independently and always assuming that $\delta = 0.6\, R_o$ as predicted from theory. It is unlikely, however, that the bubble radius R_o, the lateral film thickness δ, and the viscosity change between parts 1 and part 3 for a same explosion. From equations (9) and (18),

$$K = \frac{f_{k\delta}^2}{f_{1R_o}} = \frac{\rho_l g R_o}{2\pi\mu} \qquad (24)$$

it can be seen that viscosity μ can be determined from the knowledge of R_o, without knowing δ on which some uncertainty exists. Plotting K, calculated from "filtered" frequencies, against values of R_o obtained independently from the bubble vibrations of part 2 [*Vergniolle and Brandeis*, this issue] shows a very good correlation, except for four explosions (Figure 11b). The resulting viscosity is of 325 ± 40 Pa s, which is by far the best constrained value. Taking into account that R_o can be slightly larger, at most 15%, because of possible variations in the film thickness above the bubble cap during part 2 [*Vergniolle and Brandeis*, this issue], the viscosity may be slightly decreased, down to 275 Pa s. We therefore take the average of 300 Pa s, with a standard deviation of 65 Pa s, as the most likely value for the viscosity μ. This is in the range of values derived from petrological studies [*Shaw*, 1972; *Capaldi et al.*, 1978; *Francalanci et al.*, 1989] but with a much narrower uncertainty.

Determination of Bubble Characteristics

Similarly, combining equations (9) and (18) in another way

$$\frac{f_{1R_o}}{f_{k\delta}} = \frac{\delta}{R_o} \qquad (25)$$

provides a way of estimating δ without knowing μ. Calculating this ratio from "filtered" data shows that its

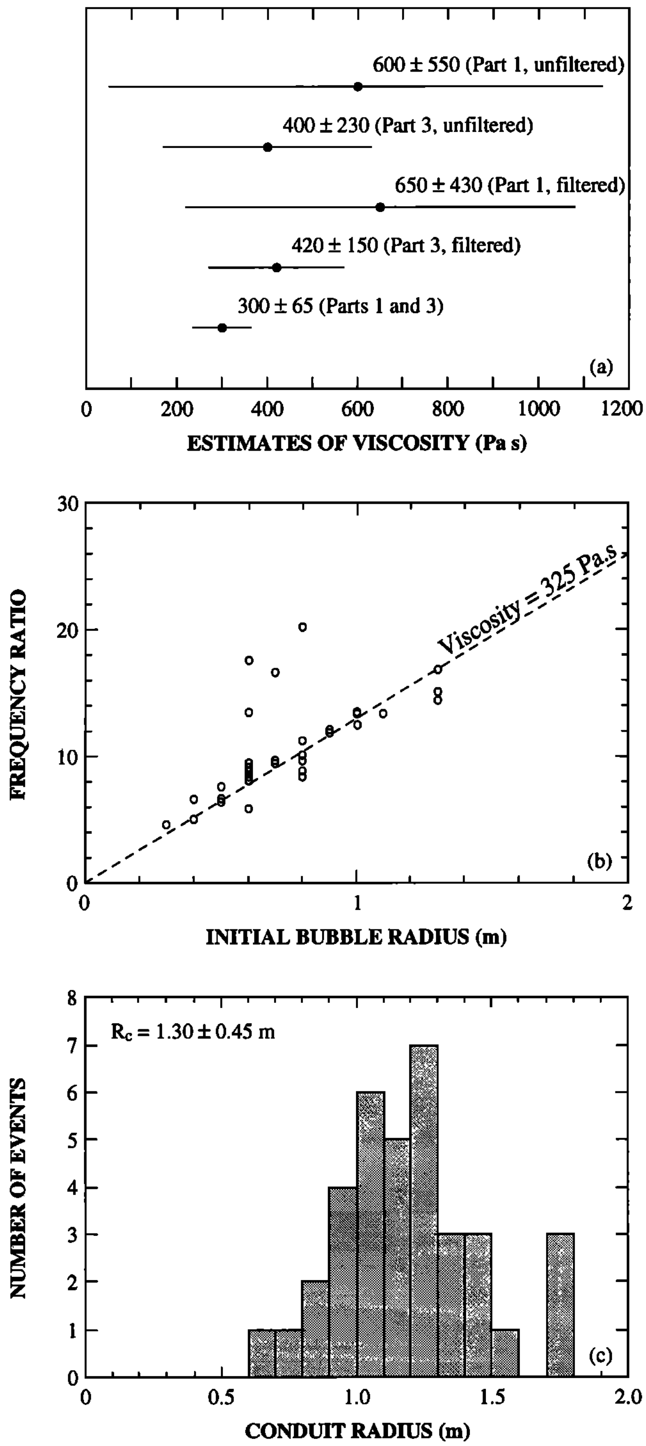

Figure 11. (a) Estimates of magma viscosity under different assumptions (see text). (b) Plot of ratio K (see text) versus bubble radius R_o determined from the bubble vibration at the surface. Straight dashed line corresponds to a magma viscosity of 325 Pa s, for a film thickness above the bubble in part 2 of 2 cm. (c) Histogram of conduit radius from bubble radius and thickness of the lateral film.

average value is 0.64 ± 0.20. This is in very good agreement with the theoretical value of 0.67 calculated for a slug flow when assuming laminar flow within the lateral film around the bubble [*Wallis*, 1969]. Taking R_o from the study of part 2 gives $\delta = 0.46 \pm 0.07$ m. Taking the average values $\mu = 300$ Pa s and $R_o = 0.9$ m, equation (10) gives the theoretical minimum film thickness $\delta_\infty = 0.28$ m, only slightly lower than the minimum we have obtained for δ, 0.3 m.

Adding the bubble radius and the thickness of the lateral film of magma gives the radius of the volcanic conduit. From above values of R_o and δ, this radius is of 1.30 ± 0.45 m (Figure 11c), in agreement with observations made inside the eastern crater in 1971 [*Chouet et al.*, 1974]. The scattering might result in part from the existence of active vents with different sizes (see above).

From equation (6) and taking previously determined values of the viscosity μ and lateral film thickness δ, the drainage velocity is 5.1 ± 1.6 m s^{-1}. Using values of bubble lengths obtained from the study of bubble vibrations in part 2, the time needed to drain the entire length of the former bubble is of the order of a few seconds, shorter but comparable to durations of eruptions estimated from analysis of videos [*Ripepe et al.*, 1993].

The good correlation between K (equation (24)) and R_o determined independently together with the excellent agreement between the theoretical and estimated thickness of lateral film reinforces the validity of our analysis associating the ≈ 4.5 Hz to kinematic waves.

Discussion

In part 3 of acoustic pressure, the amplitude spectrum shows a maximum peak around 4.5 Hz with secondary maxima around 2 and 9 Hz (Figure 7b). Audible sounds are also produced (Figure 4), for a wide variety of reasons (see above). Since frequencies of ≈ 2 Hz and ≈ 9 Hz have been produced in parts 1 and 2, respectively, a short time before part 3, their existence in part 3 could be an indirect consequence of the processes that generated them earlier. As for the ≈ 4.5 Hz mode, the ≈ 2 Hz produced at the bubble nose before it burst could have been transferred at the bottom of the bubble after its bursting by variations in the thickness of the lateral film (Figure 8). Similarly, the ≈ 9 Hz frequency may have been triggered at the bottom of the bubble by the powerful oscillation in volume of the bubble cap during part 2 but with a much lower energy (Figures 6c and 7b). These are only possible explanations, and alternate mechanisms could certainly be envisaged.

Among alternate models, *Buckingham and Garcés* [1996] consider that at Stromboli the source is explosive at depth, ≈ 100 m, and radiates sound waves in the magma which are ultimately transmitted to air. In our model, the source of vibration is shallow, a few tens of meters and does not produce sound waves in magma, although sound is generated in air by strong motions of the nearby air-magma interface.

Comparison With Seismic Records

Gas has been already thought to play an important role in generating volcanic tremors. For instance, *Chouet* [1985] suggests that an hemispherical cavity filled with gas can trigger oscillations in a buried magmatic pipe and produce tremors. At Hawaii, it was shown for long-period seismic events that tremors and gas-piston events have a similar source [*Ferrazzini and Aki*, 1992]. Recent coupled measurements of infrasonic waves with seismic waves between the explosions show that the two waves are strongly coupled [*Ripepe et al.*, 1996]. Consequently, *Ripepe et al.*, [1996] attribute the tremor at Stromboli to the regular bursting, approximately each second, of bubbles at the top of the magmatic column. However, during explosions, the bubble vibration mode at $\approx$ 9 Hz during part 2 does not appear on seismic records, although it is the most energetic on acoustic records (Figures 5d and 6c). The most likely reason is that there is no coupling between the source (i.e., the bubble cap oscillating in air) and the solid walls beneath. The proximity of these two seismic frequencies 1.9 and 3.8 Hz observed during explosion quakes and reproduced from *Dietel et al.* [1994] (Figure 5d) with those near 2 Hz and 4.5 Hz observed on acoustic records (Figure 5b) leads us to suggest that these seismic waves could be produced by the oscillation of the bubble nose when the bubble is at shallow depths and by kinematic waves along the lateral film along the conduit during part 1.

It remains to be shown that the oscillations of the bubble nose, $\approx$ 2 Hz, contain enough energy to be detected on seismic records. Assuming that the amplitude of these oscillations scales as the size of the bubble nose ($\approx$ 1 m) and taking a bubble length of several meters, the average pressure variation in the bubble is about 25% of the mean pressure, $\approx 2.0\times10^5$ Pa [*Vergniolle and Brandeis*, this issue], therefore on the order of 5×10^4 Pa. From measurements of deformation at Campi Flegrei, an active volcanic site like Stromboli, the Young modulus E is estimated to be 4×10^{10} Pa [*Russo et al.*, 1996]. The pressure variation of 5×10^4 Pa will generate deformations above 10^{-6}. For a P wave velocity of 1600 m s^{-1} at Stromboli [*Braun and Ripepe*, 1993], the wavelength is 800 m for a frequency of 2 Hz. The corresponding displacement u is equal to 10^{-3} m. Because attenuation is inversely proportional to the distance, at 300 m away from the source (assumed to be 1 m in radius), the displacement is equal to 3×10^{-6} m, still above the typical detection threshold of a seismometer and above the ground noise, 10^{-6} m, at the noisiest frequency of 0.15 Hz [*Aki and Richards*, 1980]. The same explanation could hold for the $\approx$ 4.5 Hz frequency, although the exact coupling between waves along the conduit and seismic waves in the volcanic edifice is not fully established.

Conclusion

In this paper and its companion [*Vergniolle and Brandeis*, this issue], we have proposed to relate variations in acoustic pressure at Stromboli to the behavior of a large bubble rising in the volcanic conduit and breaking at the air-magma interface. We have identified three phases on acoustic pressure records and related each phase to a specific type of oscillations. The first part of the signal is mostly due to oscillations of the bubble nose, at $\approx$ 2 Hz, when it is approaching the surface and one could "hear" a bubble travelling in the uppermost 30 m of the magma column. The second part, the most energetic, is due to the vibration of this bubble at the interface, at $\approx$ 9 Hz. After the bubble bursts, kinematic waves develop along the vertical film of magma draining on the conduit walls and generate frequencies of $\approx$ 4.5 Hz.

Our interpretation is based on reasonable mechanisms, bubble vibrations and slug flow, which have been observed and studied before. Hence we have been able to derive some physical characteristics of the magma and the conduit. From the bubble vibration during part 2, we have constrained the bubble radius to be of the order of 0.9 m, compatible with independent determinations. From this value we have estimated the thickness of the lateral film of magma to be 0.46 ± 0.07 m, in excellent agreement with theoretical studies of viscous slug flow. We also have obtained a robust constraint on the magma viscosity by combining results. From the spectral analysis of parts 1 and 3 and modeling of the bubble vibration mode, we have obtained a viscosity of 300 ± 65 Pa s, in agreement with petrological modeling but in a much narrower range.

The fact that the $\approx$ 2 Hz and $\approx$ 4.5 Hz frequencies are observed both on acoustic and seismic records leads us to propose that bubble vibrations could be a source of seismicity as well as airborne sound. Combining seismic and acoustic measurements would certainly help to distinguish shallow sources, linked to degassing phenomena, from deeper events in the seismic records and thus provide valuable informations on the dynamics of volcanic eruptions.

Acknowledgments. We thank X. Hill, G. Sartoris, V. Ferrazini, P. Allard, C. Bercy, D. Bréfort, R. Verhille, G. Bienfait, M. Martini, F. Barberi, H. Lyon-Caen, P. Briole, Y. Gaudemer, T. Trull, M.-F. Le Cloarec, S. Cardoso. Thorough reviews by R. S. J. Sparks, M. J. Buckingham, and T. Koyaguchi greatly improved the manuscript. This work was supported by CNRS-INSU-DBT Terre profonde and EEC grants SC1*CT005010 and EV5V-CT92-0189. This is IPGP Contribution 1442 and INSU-DBT contribution 765.

References

Aki, K., and P. G. Richards, *Quantitative Seismology: Theory and Methods*, vol. 1, 557 pp., W. H. Freeman, New York, 1980.

Batchelor, G. K., *An Introduction to Fluid Dynamics*, 615 pp., Cambridge Univ. Press, New York, 1967.

Bercy, C., J.-C. Sabroux, and G. Suparwoto, Underwater noise survey in the crater lake of Kelut volcano (Indoneasia), in *Development in Volcanology: Forecasting Volcanic Events*, edited by H. Tazieff and J.-C. Sabroux, pp. 529–543, Elsevier, New York, 1983.

Blackburn, E. A., L. Wilson, and R. S. J. Sparks, Mechanics and dynamics of Strombolian activity, *J. Geol. Soc. London*, *132*, 429–440, 1976.

Bottinga, Y., and D. F. Weill, The viscosity of magmatic silicate liquids: a model for calculation, *Am. J. Sci.*, *272*, 438–475, 1972.

Braun, T., and M. Ripepe, Interaction of seismic and air waves recorded at Stromboli volcano, *Geophys. Res. Lett.*, *20*, 65–68, 1993.

Buckingham, M. J., and M. A. Garcés, Canonical model of volcano acoustics, *J. Geophys. Res.*, *101*, 8129–8151, 1996.

Capaldi, G., et al., Stromboli and its 1975 eruption, *Bull. Volcanol.*, *41*, 1–27, 1978.

Chouet, B., Excitation of a buried magmatic pipe: a seismic source model for volcanic tremor, *J. Geophys. Res.*, *90*, 1881–1893, 1985.

Chouet, B., N. Hamisevicz, and T. R. McGetchin, Photoballistics of volcanic jet activity at Stromboli, Italy, *J. Geophys. Res.*, *79*, 4961–4975, 1974.

Del Pezzo E., C. Godano, A. Gorini and M. Martini, Wave polarisation and the location of the source of the explosion quakes at Stromboli volcano, in *Volcanic Seismology*, edited by P. Gasparini, R. Scarpa, and K. Aki, pp. 279–296, Springer-Verlag, New York, 1992.

Dietel, C., B. Chouet, J. Kleinman, G. de Luca, M. Martini, G. Milana, J. Power, D. Harlow, and R. Scarpa, Array tracking of tremor sources at Stromboli volcano, Italy, *U.S. Geol. Surv. Open File Rep.94-142*, 1994.

Donn, W. L., and N. K. Balachandran, Mount St. Helens eruption of 18 May 1980: Air waves and explosive yield, *Science*, *213*, 539–541, 1981.

Fabre, J., and A. Linné, Modelling of two-phase slug flow, *Annu. Rev. Fluid Mech.*, *24*, 21–46, 1992.

Ferrazzini, V., and K. Aki, Preliminary results from a field experiment on volcanic events at Kilauea using an array of digital seismographs, *IAVCEI Proc. Volcanol.*, *3*, 168–189, 1992.

Francalanci, L., P. Manetti, and A. Pecerillo, Volcanological and magmatological evolution of Stromboli volcano (Aeolian islands): The roles of fractional crystallization, magma mixing, crustal contamination, and source heterogeneity, *Bull. Volcanol.*, *51*, 335–378, 1989.

Gaonac'h, H., J. Vandemeulebrouck, J. Stix, and M. Halbwachs, Thermal infrared satellite measurements of volcanic activity at Stromboli and Vulcano, *J. Geophys. Res.*, *99*, 9477–9485, 1994.

Giberti, G., C. Jaupart, and G. Sartoris, Steady-state operation of Stromboli volcano, Italy: Constraints on the feeding system, *Bull. Volcanol.*, *54*, 535–541, 1992.

Golstein, P., and B. Chouet, Array measurements and modeling of sources of shallow volcanic tremor at Kilauea volcano, Hawaii, *J. Geophys. Res.*, *99*, 2637–2652, 1994.

Jaupart, C., and S. Vergniolle, Dynamics of degassing at Kilauea volcano, Hawaii, *Nature*, *331*, 58–60, 1988.

Jaupart, C., and S. Vergniolle, The generation and collapse of a foam layer at the roof of a basaltic magma chamber, *J. Fluid Mechanics*, *203*, 347–380, 1989.

Kanamori, H., and J. W. Given, Analysis of long-period seismic waves ecited by the May 18, 1980, eruption of Mount St. Helens: A terrestrial monopole, *J. Geophys. Res.*, *87*, 5422–5432, 1982.

Kanamori, H., and J. Mori, Harmonic excitation of mantle Rayleigh waves by the 1991 eruption of Mount Pinatubo, Philippines, *Geophys. Res. Lett.*, *19*, 721–724, 1992.

Kanamori, H., J. W. Given, and T. Lay, Analysis of seismic body waves by the Mount St. Helens eruption of May 1980, *J. Geophys. Res.*, *89*, 1856–1866, 1984.

Kieffer, S. W., and B. Sturtevant, Laboratory studies of volcanic jets, *J. Geophys. Res.*, *89*, 8253-8268, 1984.

Kinsler, L. E., A. R. Frey, A. B. Coppens, and J. V. Sanders, *Fundamentals of Acoustics*, 480 pp., John Wiley, New York, 1982.

Landau, L. D., and E. M. Lifshitz, *Course in Theoretical Physics: Fluids Mechanics*, vol. 6, 536 pp., Pergamon, Tarrytown, N.Y., 1987.

Leighton, T.G., *The Acoustic Bubble*, 613 pp., Academic, San Diego, Calif., 1994.

Lighthill, J., *Waves in Fluids*, 504 pp., Cambridge Univ. Press, New York, 1978.

Lo Bascio A., G. Luongo, and G. Nappi, Microtremors and volcanic explosions at Stromboli (Aeolian Islands), *Bull. Volcanol.*, *37*, 596–606, 1973.

Machado, F., W. H. Parsons, A. F. Richards, and J. W. Mulford, Capelinhos eruption of Fayal volcano, Azores, 1957-1958, *J. Geophys. Res.*, *67*, 3519–3529, 1962.

Mikumo, T., and B. A. Bolt, Excitation mechanism of atmospheric pressure waves from the 1980 Mount St. Helens eruption, *Geophys. J. R. Astron. Soc.*, *81*, 445–461, 1985.

Neuberg, J., R. Luckett, M. Ripepe, and T. Braun, Highlights from a seismic broadband array on Stromboli, *Geophys. Res. Lett.*, *21*, 749–752, 1994.

Norris, R. A., and R. H. Johnson, Submarine volcanic eruptions recently located in the pacific by sofar hydrophones, *J. Geophys. Res.*, *74*, 650–664, 1969.

Ntepe, N., and J. Dorel, Observations of seismic volcanic signals at Stromboli volcano, Italy, *J. Volcanol. Geotherm. Res.*, *43*, 235–251, 1990.

Paterson, A. R., *A First Course in Fluid Dynamics*, 528 pp., Cambridge Univ. Press, New York, 1983.

Pierce, A. D., *Acoustics: An Introduction to Its Physical Principles and Applications*, 678 pp., McGraw-Hill, New York, 1981.

Richards, A. F., Volcanic sounds, investigation and analysis, *J. Geophys. Res.*, *68*, 919–928, 1963.

Ripepe, M., M. Rossi, and G. Saccarotti, Image processing of explosive activity at Stromboli, *J. Volcanol. Geotherm. Res.*, *54*, 335–351, 1993.

Ripepe, P. Poggi, T. Braun, and E. Gordeev, Infrasonic waves and volcanic tremor at Stromboli, *Geophys. Res. Lett.*, *23*, *2*, 181–184, 1996.

Roscoe, R., The viscosity of suspensions of rigid spheres, *J. Br. Appl. Phys.*, *3*, 267–269, 1952.

Russo, G., G. Giberti, and G. Sartoris, The influence of regional stresses on the mechanical stability of volcanoes: Stromboli (Italy), in *Volcano Instability on the Earth and Other Planets*, Spec. Pub. Geol. Soc., 110, 65–75, 1996.

Settle, M., and T. R. McGetchin, Statistical analysis of persistent explosive activity at Stromboli, 1971: Implications for eruption predictions, *J. Volcanol. Geotherm. Res.*, *8*, 45–58, 1980.

Shaw, H. R., Viscosities of magmatic silicate liquids: An empirical method of prediction, *Am. J. Sci.*, *272*, 870–893, 1972.

Sparks, R. S. J., The dimensions and dynamics of volcanic eruption columns, *Bull. Volcanol.*, *56*, 493–501, 1986.

Swanson, D. A., W. A. Duffield, D. B. Jackson, and D. W. Peterson, Mauna Ulu eruption, Kilauea volcano, *Geotimes*, *16*, 12–16, 1971.

Taylor, G. I., and R. M. Davies, The motion and shape of the hollow produced by an explosion in a liquid, *The Scientific Papers of G.I. Taylor, vol. 3*, pp. 337–353, Cambridge Univ. Press, New York, 1963.

Vandemeulebrouk J., A. W. Hurst, and N. Poussielgue, Implications for the thermal regime of acoustic noise measurements in Crater Lake, Mount Ruapehu, New Zealand, *Bull. Volcanol.*, *56*, 493–501, 1994.

Vergniolle, S., and G. Brandeis, Origin of the sound generated by Strombolian explosions, *Geophys. Res. Lett.*, *21*, 1959–1962, 1994.

Vergniolle, S., and G. Brandeis, Strombolian explosions, 1, A large bubble breaking at the surface of a lava column as a source of sound, *J. Geophys. Res.*, this issue.

Vergniolle, S., and C. Jaupart, The dynamics of degassing at Kilauea volcano, Hawaii, *J. Geophys. Res.*, *95*, 2793–2809, 1990.

Wallis, G. B., *One Dimensional Two-Phase Flows*, 408 pp., McGraw-Hill, New York, 1969.

Weill, A., G. Brandeis, S. Vergniolle, F. Baudin, J. Bilbille, J.-F. Fèvre, B. Piron, and X. Hill, Acoustic sounder measurements of the vertical velocity of volcanic jets at Stromboli volcano, *Geophys. Res. Lett.*, *19*, 2357–2360, 1992.

Whitham, G. B., *Linear and Nonlinear Waves*, 636 pp., John Wiley, New York, 1973.

Wilson, L., Relationships between pressure, volatile content and ejecta velocity, *J. Volcanol. Geotherm. Res.*, *8*, 297–313, 1980.

Wilson, L., and J. W. Head, Ascent and eruption of basaltic magma on the Earth and Moon, *J. Geophys. Res.*, *86*, 2971–3001, 1981.

Wilson, L., R. S. J. Sparks, T. C. Huang, and N. D. Watkins, The control of volcanic column heights by eruption energetics and dynamics, *J. Geophys. Res.*, *83*, 1829–1835, 1978.

Woods, A.W., The fluid dynamics and thermodynamics of eruption columns, *Bull. Volcanol.*, *50*, 169–193, 1988.

Woulff, G., and T.R. McGetchin, Acoustic noise from volcanoes: Theory and experiments, *Geophys. J. R. Astron. Soc.*, *45*, 601–616, 1976.

G. Brandeis, UMR 5562/CNRS, GRGS, Observatoire Midi-Pyrénées, 14 avenue Edouard-Belin, 31400 Toulouse, France. (e-mail: brandeis@pontos.cst.cnes.fr)

J.-C. Mareschal, GEOTOP, Université du Québec à Montréal, Case postale 8888, Montréal, H3C 3P8, Québec, Canada. (e-mail: jcm@volcan.geotop.uqam.ca)

S. Vergniolle, Laboratoire de Dynamique des Systèmes Géologiques, Institut de Physique du Globe, 4 place Jussieu, 75252 Paris cedex 05, Paris, France. (e-mail:vergniol@ipgp.jussieu.fr)

(Received June 13, 1995; revised April 29, 1996; accepted June 4, 1996.)